The Integrated Photon Echo and Solvation Dynamics

Minhaeng Cho[†]

Department of Chemistry, Massachusetts Institute of Technology, Cambridge, Massachusetts 02139

Jae-Young Yu, Taiha Joo,[‡] **Yutaka Nagasawa, Sean A. Passino, and Graham R. Fleming***

Department of Chemistry and the James Franck Institute, The University of Chicago, Chicago, Illinois 60637

Received: January 22, 1996; In Final Form: May 6, 1996[⊗]

The time-integrated three-pulse photon echo is discussed in terms of the line-shape functions which are shown to be directly related to the solvation dynamics. By using the short-time approximation to the line-shape function, an algebraic form of the three-pulse photon echo signal $S_{PE}(\tau, T)$ is obtained as a function of two delay times, τ and T, between pulses. On the basis of the approximate form of the photon echo signal, the echo peak shift with respect to the second delay time (population evolution period) is derived and found to be linearly proportional to the time-dependent fluorescence Stokes shift function for times greater than the bath correlation time, τ_c. In the case of intermediate inhomogeneous broadening, the asymptotic echo peak shift magnitude is found to be useful in estimating the static inhomogeneous width. To illustrate the theoretical results, an analysis of the echo peak shift measurement of IR144 in a room temperature glass, PMMA, is presented.

I. Introduction

It has usually been assumed that the broad Gaussian shape of the optical spectrum originates from a distribution of the static local environments around the chromophores.[1,2] This static limit holds when impurity chromophores are dissolved in a medium such as glasses, since in these cases the typical time scale of the transitions from one local structure to another is extremely slow in comparison to that of the phonon fluctuation correlation function. In the case of the ideal large inhomogeneous broadening limit, photon echo measurements have been used to effectively eliminate the inhomogeneous contribution to the optical spectrum.[3−9] It is the rephasing of the optical coherence that generates the coherent echo field, the decay of which represents the homogeneous dephasing process induced by the fluctuating bath degrees of freedom.[10,11]

The situation in liquid solutions is more complex. The time scale of local structural transitions ranges from a few picoseconds to hundreds of picoseconds, and these processes are responsible for the slowly decaying portion of the bath correlation function. On time scales longer than these, liquids are not expected to exhibit inhomogeneity. Thus, the standard picture of echo formation as a result of static inhomogeneity is inappropriate in liquids. At short times inertial motions play a dominant role in solvation dynamics, at least in small highly polar liquids.[12−15] This Gaussian relaxation caused by inertial motions of solvent acts as an inhomogeneous contribution to the echo signal at short time, giving rise to Gaussian spectral broadening in the frequency domain. Even when there is a static inhomogeneous contribution, if its width is comparable to, or smaller than, the inverse of the bath correlation time, τ_c, it is difficult to completely eliminate the inhomogeneous contribution in two-pulse photon echo measurements. Considerations such as these led Cho *et al.* to suggest the heterodyne-detected stimulated photon echo[16] and the fifth-order three-pulse photon echo experiments,[17] and recently these new types of experiments have been performed by Wiersma and co-workers[18] and Fleming and co-workers,[19] respectively. Closely related time-gated photon echo measurements[20,21] have also been found useful in measuring the nonlinear response of the bath. All these studies revealed more detailed information on the dynamics of line broadening in condensed media than was available from conventional photon echo measurements.

In parallel to the echo studies a great deal of activity has been devoted to solvation dynamics via fluorescence Stokes shift measurements,[14,15] computer simulations,[13,22] and theory.[11,23−26] However, the connection of these studies to echo spectroscopy has not been clearly established, and frequently echo studies have been analyzed at a phenomenological level. An experimental approach described by Weiner *et al.*,[27] namely, that of recording the shift of the echo peak from zero delay, in a time-integrated third-order three-pulse photon echo has recently been investigated by Joo *et al.*[28] By means of numerical simulations, they were able to show that the echo peak shift was closely related to the solvation dynamics, which are in turn connected to the homogeneous bath fluctuations. In this paper we will establish this connection formally and show that the echo peak shift with respect to the second delay period, T (see Figure 1), is linearly proportional to the solvation correlation function in the long-time region. We will also show how the inhomogeneous width can be obtained from peak shift measurements.

This paper is organized as follows: In section II, the general aspects of the nonlinear response functions are discussed after a general model Hamiltonian is introduced. We next discuss the solvation correlation function and its connection to the line-shape function via the definition of the spectral density. By using a short-time approximation, an approximate time-integrated photon echo signal is derived in section IV. The relationship between the echo peak shift and solvation correlation function is discussed in section V. An analysis of the echo shift measurement of IR144 in a room temperature glass, PMMA, is presented to illustrate the theoretical results devel-

* Corresponding author. E-mail address: fleming@femto.uchicago.edu.
† Present address: Department of Chemistry, Korea University, 1, Anam-dong, Seoul, 136-701, Korea.
‡ Present address: Department of Chemistry, Pohang University of Science and Technology, Pohang, 790-784, Korea.
⊗ Abstract published in *Advance ACS Abstracts,* July 1, 1996.

S0022-3654(96)00198-0 CCC: $12.00

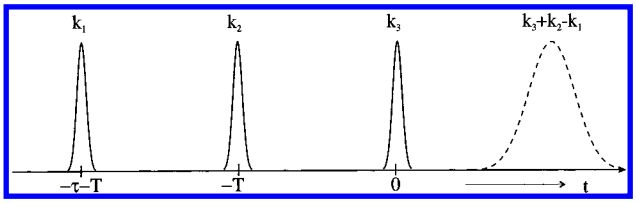

Figure 1. Pulse sequences of the three-pulse photon echo. Three consecutive pulses with wave vectors of $\mathbf{k}_1$, $\mathbf{k}_2$, and $\mathbf{k}_3$ are separated by τ and T. The echo field generated by the rephasing process is pictorially shown by the last peak. From the phase matching condition, the wave vector of the photon echo field is $\mathbf{k}_3 + \mathbf{k}_2 - \mathbf{k}_1$. The integrated photon echo is measured by integrating the photon echo intensity along this direction.

oped in this paper. We summarize the results with some concluding remarks in section VII.

II. Nonlinear Response Functions

An optical chromophore dissolved in a condensed medium is often modeled by assuming a two-electronic-state system coupled to the bath degrees of freedom in addition to the external electric fields. The contribution from the intramolecular modes to the photon echo signal has been found to be important by Wiersma and co-workers[8] and Shank and co-workers,[7] and it is straightforward to incorporate the intramolecular modes into the displaced harmonic oscillator model, by adding properly weighted spikes into the total spectral density representing the coupling strength and distribution of harmonic oscillators. For the sake of simplicity, we assume that there are no strongly coupled intramolecular modes of the chromophore to the optical excitation. Consequently, the oscillatory features of the optical broadening function are not considered in this paper. An extensive discussion of the intramolecular vibrational mode contributions to the photon echo and other four-wave mixing spectroscopies is given by Joo *et al.*[28]

A two-state system coupled to both the bath degrees of freedom and external optical fields can be, in general, described by the following Hamiltonian

$$H = {}^1/_2\hbar\Omega\sigma + \mu\cdot\mathbf{E}(\mathbf{r},t)\sigma_x + {}^1/_2\sigma_z V_{SB}(\{q_\alpha\},Q) + H_B(\{p_\alpha,q_\alpha\},Q) \quad (1)$$

where the Pauli matrices are denoted by σ's and μ is the electronic dipole matrix element. Ω is the electronic transition frequency. The third term on the right-hand side of eq 1 represents the coupling potential among the bath coordinates $\{q_\alpha\}$, chromophore coordinate Q, and the optical transition. The specific functional form of the coupling potential $V_{SB}(\{q_\alpha\},Q)$ is determined by the bath model that one is interested in. Note that the system−bath coupling is diagonal so that within this model Hamiltonian the optical transition frequency is modulated by the bath degrees of freedom via the coupling potential $V_{SB}(\{q_\alpha\},Q)$, but there is no electronic transition induced by the bath fluctuations. $\mathbf{E}(\mathbf{r},t)$ is the external electric field including three distinct optical fields in the case of four-wave mixing spectroscopies. We use the semiclassical approximation to the field−matter interaction, though its quantum generalization of the field is straightforward.[29] As long as the intensity of the optical field is high enough to ignore the photon number distribution of the field—the photon number distribution is narrow so that the average photon number is the only relevant parameter determining the field amplitude—a classical treatment of the electric field should be appropriate. $H_B(\{p_\alpha,q_\alpha\},Q)$ represents the Hamiltonian describing the initial equilibrium state of the system. Depending on the line broadening model, for example the Brownian oscillator or the effective harmonic bath models, the bath Hamiltonian may depend on the optically active system coordinate,[29] where the system coordinate is fully in equilibrium with the bath degrees of freedom initially.

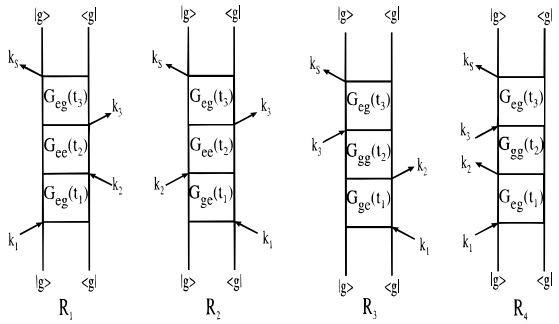

Figure 2. Four double-sided Feynman diagrams associated with the four nonlinear response functions given in eq 2. The arrows represent the interaction with the external fields with wave vectors $\mathbf{k}_1$, $\mathbf{k}_2$, and $\mathbf{k}_3$. $G_{ij}(t)$ and $G_{ii}(t)$ describe the time evolution of off-diagonal and diagonal elements of a density matrix, respectively.

For the given Hamiltonian, eq 1, the photon echo signal, which is fourth-order with respect to the field−chromophore interaction, can be most easily described by using the nonlinear response function formulation. The density operator can be perturbatively expanded to obtain the third-order density operator. Then the polarization of the optical sample can be calculated from the expectation value of the electric dipole operator traced over the third-order density operator. Since the third-order density operator depends on four time arguments, one can obtain the photon echo polarization in terms of the nonlinear response functions with three time variables which represent time differences between the consecutive time arguments. References 17 and 30 give a detailed description of the photon echo polarization expressed as a triple integral over the three time differences. Although in general the associated nonlinear response functions depend on three time differences *independently*, when the fluctuating coupling potential $V_{SB}(\{q_\alpha\},Q)$ obeys Gaussian statistics, they can be expressed in terms of simple line-shape functions, $g(t)$. $g(t)$ defined in this manner includes only the contributions to line broadening from dynamical processes. In general, the actual spectral line shape may also contain a static contribution. One of the advantages of rewriting the nonlinear response functions in terms of line-shape functions is that the latter functions are simple two-time correlation functions depending on a single time difference. Those four third-order response functions are[29]

$$R_1(t_3,t_2,t_1) = \exp[-g(t_1) - g^*(t_2) - g^*(t_3) + g(t_1+t_2) + g^*(t_2+t_3) - g(t_1+t_2+t_3)]$$

$$R_2(t_3,t_2,t_1) = \exp[-g^*(t_1) + g(t_2) - g^*(t_3) - g^*(t_1+t_2) - g(t_2+t_3) + g^*(t_1+t_2+t_3)]$$

$$R_3(t_3,t_2,t_1) = \exp[-g^*(t_1) + g^*(t_2) - g(t_3) - g^*(t_1+t_2) - g^*(t_2+t_3) + g^*(t_1+t_2+t_3)]$$

$$R_4(t_3,t_2,t_1) = \exp[-g(t_1) - g(t_2) - g(t_3) + g(t_1+t_2) + g(t_2+t_3) - g(t_1+t_2+t_3)] \quad (2)$$

The corresponding double-sided Feynman diagrams are shown in Figure 2. The line-shape function, $g(t)$, is determined by

the autocorrelation function of the fluctuating part of the coupling potential, $\delta V_{SB}(t) = V_{SB}(t) - \langle V_{SB}\rangle$, as

$$g(t) = \frac{1}{\hbar^2}\int_0^t d\tau \int_0^\tau d\tau' \, \langle \delta V_{SB}(\tau')\delta V_{SB}(0)\rangle \tag{3}$$

$\delta V_{SB}(t)$ is the Heisenberg operator of δV_{SB}. The Heisenberg operator is chosen to propagate under the ground electronic state Hamiltonian. This is a semiclassical approximation, but as Shemetulskis and Loring show,[31] other choices such as the arithmetic mean of ground and excited Hamiltonians make only small differences in the predicted dynamics, except in pathological cases. Since the integrand of eq 3 is a one-sided quantum correlation function, the line-shape function is complex. The real part of the line-shape function is thus responsible for the optical broadening effect, whereas the imaginary part describes time-dependent spectral diffusion, for example, the time-dependent fluorescence Stokes shift. At this stage, one probably needs to introduce an appropriate model for the coupling potential operator, which is a difference potential operator modulating the optical transition frequency. In the Brownian oscillator model,[29,30,32,33] the fluctuating coupling potential is linearly proportional to a single harmonic oscillator coordinate, which is in turn coupled to the bath degrees of freedom. Because of the couplings between the optically active main oscillator and the bath degrees of freedom, the equation of motion for the main oscillator becomes the generalized Langevin equation with a time-nonlocal damping kernel. On the other hand, if one uses an effective harmonic oscillator bath model, where a collection of harmonic oscillators are linearly coupled to the optical transition, the fluctuating coupling potential δV_{SB} becomes linearly proportional to the coordinates of every oscillator with appropriate coupling constants. We shall show in the next section that the *spectral density* representation of the bath dynamics can be used for an arbitrary model bath, e.g., the Brownian oscillator model, the bosonic bath model, etc.

III. Solvation Dynamics and Line-Shape Function

Four-wave mixing spectroscopies, including photon echo measurements, are completely described by the four nonlinear response functions discussed in section II, which are in turn determined by the line-shape function $g(t)$. It is often assumed that the autocorrelation function of the fluctuating coupling potential can be replaced with the classical correlation function. However, in this case the spectral diffusion, associated with the imaginary part of the line-shape function, cannot be included in the nonlinear spectroscopy. For example, Cho and Fleming[34] studied the photon echo phenomena by replacing the normalized autocorrelation function, $\langle \delta V_{SB}(t)\delta V_{SB}(0)\rangle/\langle \delta V_{SB}{}^2\rangle$, with the time-dependent fluorescence Stokes shift function. It has been speculated that in the classical (high-temperature) limit the procedure mentioned above is quantitatively correct. In this section, we present a more rigorous discussion of how these correlation functions are related to one another.

We first consider the time-dependent fluorescence Stokes shift (FSS) function defined as

$$S(t) = \frac{\Delta\bar{E}(t) - \Delta\bar{E}(\infty)}{\Delta\bar{E}(0) - \Delta\bar{E}(\infty)} \tag{4}$$

where $\Delta\bar{E}(t)$ is the nonequilibrium energy difference between the excited state and the ground state and is proportional to the central frequency of the time-dependent fluorescence spectrum. Since the initial population created on the electronic excited state is in a (quasi) nonequilibrium state on the potential surface of the excited state, the FSS function defined above reflects the relaxation of the nonequilibrium state. To establish the relationship between the nonequilibrium relaxation and fluctuation correlation in the equilibrium state, one can divide the energy difference operator ΔE into two parts, i.e.,

$$\Delta E = \langle \Delta E\rangle + \delta V_{SB} \tag{5}$$

where $\langle \Delta E\rangle$ is the average transition energy calculated over the ensemble of the chromophores. Therefore, the distribution of the static local environments around the chromophores is taken into account by this average value. The fluctuating coupling potential is thus the fluctuating part of the energy difference operator. With the definitions of the FSS function and the energy difference operator in eq 5 and by using the linear response theory, the nonequilibrium quantity $\Delta\bar{E}(t)$ can be most generally written by an integral over the response function.[35] Then the FSS function, $S(t)$, becomes

$$S(t) = \frac{\int_t^\infty d\tau \, G(\tau)}{\int_0^\infty d\tau \, G(\tau)} \tag{6}$$

where the response function $G(t)$ is defined as a mean value of the commutator of the Heisenberg operator $\delta V_{SB}(t)$, the fluctuating coupling potential,[35]

$$G(t) = \frac{i}{\hbar}\langle [\delta V_{SB}(t), \delta V_{SB}(0)]\rangle \tag{7}$$

In addition to the antisymmetrized correlation function, we define the symmetrized correlation function as $C(t)$,

$$C(t) = \frac{1}{\hbar}\langle \{\delta V_{SB}(t), \delta V_{SB}(0)\}\rangle \tag{8}$$

As we shall show later, it is very convenient to introduce the spectral density defined as

$$\rho(\omega) \equiv \frac{2}{\pi\hbar}\frac{\mathrm{Im}[\tilde{G}(\omega)]}{\omega^2} \tag{9}$$

where $\tilde{G}(\omega)$ is the Fourier−Laplace transform of the response function,

$$\tilde{G}(\omega) = \int_0^\infty dt \, e^{i\omega t} \, G(t) \tag{10}$$

From now on, we shall use the definition of the spectral density in eq 9 to express various correlation functions relevant to the optical spectroscopic broadening and spectral diffusion.

For example, the fluorescence Stokes shift function S(t) can be rewritten in terms of the spectral density as

$$S(t) = \frac{\hbar}{\lambda}\int_0^\infty d\omega \, \omega\rho(\omega) \cos \omega t \tag{11}$$

where the normalization constant λ is identical to the solvation reorganization energy,

$$\lambda = \hbar\int_0^\infty d\omega \, \omega\rho(\omega) \tag{12}$$

From eqs 11 and 12, the physical meanings of the Stokes shift and reorganization energy become clear in the spectral density representation. The first moment of the spectral density, multiplied by Planck's constant, is equal to the reorganization energy, and the time-dependent change of the first moment corresponds to the time-dependent fluorescence Stokes shift,

where the time dependence of the FSS function is completely determined by the spectral density once it is known.

Before we discuss the connection between the FSS function $S(t)$, and the line-shape function $g(t)$, it is useful to consider the classical limit of the time-dependent fluorescence Stokes shift, eq 6. In this limit, where the spectral distribution of the fluctuation is far less than $2k_BT$, the response function is directly related to the classical correlation function by[36]

$$G_{cl}(t) = -\beta \frac{d}{dt} C_{cl}(t) = -\beta \frac{d}{dt} \langle \delta V_{SB}(t) \delta V_{SB}(0) \rangle_{cl} \quad (13)$$

where the average is taken over the classical phase space and δV_{SB} is a classical variable not an operator. $\beta = 1/k_BT$ where k_B is the Boltzmann constant and T is the absolute temperature. Using this classical fluctuation−dissipation relation in the definition of the fluorescence Stokes shift function in eq 6, the well-known relationship between the FSS (solvation) function and the classical correlation function of the fluctuation can be recovered

$$S(t) = \frac{\langle \delta V_{SB}(t) \delta V_{SB}(0) \rangle_{cl}}{\langle \delta V_{SB}{}^2 \rangle_{cl}} \quad (14)$$

Equation 14 is a formal expression of Onsager's regression hypothesis in the classical limit.

We next focus on the line-shape function, $g(t)$, in the spectral density representation. From the definitions of the antisymmetrized and symmetrized correlation functions of the fluctuating coupling potential, the line-shape function can be rewritten as

$$g(t) = \frac{1}{2\hbar} \int_0^t d\tau \int_0^\tau d\tau' \{C(\tau') - iG(\tau')\} \quad (15)$$

Generally, the symmetrized correlation function $C(t)$ is not simply related to the response function $G(t)$ via a time-derivative relation, eq 13 of the classical limit. In the classical limit, the temperature is the only bath parameter determining the fluctuation−dissipation relation.[36] On the other hand, in the case of a general quantum system, the quantum fluctuation−dissipation relation shows that the relation between the symmetrized and antisymmetrized correlation functions of the fluctuation requires a complete knowledge of the spectral distribution of the fluctuation, i.e., $\rho(\omega)$.[35] Again the spectral density defined in eq 9 plays a key role in describing the line-shape function:

$$g(t) = -i\lambda t/\hbar + \int_0^\infty d\omega\, \rho(\omega) \coth[\hbar\omega\beta/2](1 - \cos \omega t) + i\int_0^\infty d\omega\, \rho(\omega) \sin \omega t \quad (16)$$

From eqs 11 and 16, it should be clear how the fluorescence Stokes shift function $S(t)$ is related to the optical line-shape function $g(t)$ via the spectral density. The spectral density scaled by λ can be obtained by the cosine transformation of the time-dependent FSS or solvation correlation function provided the Stokes shift magnitude (i.e., 2λ) is also known. One can use either theoretical methods[12,23−26] or computer simulation techniques[13,22] to obtain the solvation correlation function in parallel with the experimental fluorescence Stokes shift measurements. Using the spectral density thus obtained, the optical line-shape function can be completely evaluated and eventually the nonlinear response function can be constructed by using eq 2. One can also use the reverse procedure to obtain some information on the solvation dynamics by using time-domain nonlinear spectroscopic methods. It is one of our goals in this paper to show that *photon echo peak shift measurements can be used to study solvation dynamics in liquids.*

We close this section by emphasizing that the above discussion is in fact quite general and valid regardless of the bath model used as long as the system−bath coupling is diagonal with respect to the electronic basis. Any arbitrary bath model can be incorporated into the spectral density representation with the appropriate functional form.

IV. Approximate Integrated Photon Echo Signal in the Impulsive Limit

As discussed in section II, the photon echo signal is proportional to the square of the third-order optical polarization within the slow-varying-amplitude approximation. The third-order polarization, which acts as a source term generating the electric field from the sample, can be fully described by the nonlinear response functions listed in eq 2. Instead of considering a general case with finite pulse width, we will assume that the pulse width is short enough to replace the time profile of the pulses with delta functions. This cannot be justified when the bath has dynamical time scales on the order of the width of the optical pulse. However, remarkable developments in ultrashort laser design allow routine generation of 10−20 fs pulses. Such pulses can often be approximated as delta functions. Effects caused by the finite width of optical pulses can be studied by using numerical methods and will be discussed briefly in the following sections. Referring to Figure 1, the first and the second delay times are denoted by τ and T, respectively. When the three wave vectors associated with the consecutive three pulses are $\mathbf{k}_1$, $\mathbf{k}_2$, and $\mathbf{k}_3$, respectively, the echo field is generated with a wave vector of $\mathbf{k}_3 + \mathbf{k}_2 - \mathbf{k}_1$, because of the phase-matching condition. In Figure 1, the last peak is a pictorial representation of the echo field emitted by the sample after some time t from the last pulse.

In the impulsive limit, the third-order photon echo signal becomes

$$S_{PE}(\tau, T) \propto \int_0^\infty dt\, I(t-\tau) \exp[-2\{P(\tau) - P(T) + P(t) + P(\tau + T) + P(T + t) - P(\tau + T + t)\}] \cos^2[Q(T) + Q(t) - Q(T + t)] \quad (17)$$

where $P(t)$ and $Q(t)$ are the real and the imaginary part of the line-shape function, respectively. $I(t-\tau)$ represents the inhomogeneous contribution to the nonlinear response functions:

$$I(t-\tau) = \exp[-\Delta_{in}{}^2 (t - \tau)^2] \quad (18)$$

Here, Δ_{in} represents the width of the inhomogeneous distribution of the static environment. In many liquids, the inhomogeneous contribution will be zero, i.e., $\Delta_{in} = 0$, since there are no static environments. Although it is straightforward to calculate eq 17, we find that it is more useful to evaluate the integral using the Laplace method. As can be seen in the Feynman diagrams, during the last time period, t, the chromophore evolves in on electronic coherence, which is quickly destroyed by the fast dephasing process. Therefore, the exponential term inside of the integrand of eq 17 is a very quickly varying function with respect to t, so we can use a short-time approximation to the P and Q functions in eq 17 with respect to t only. The cosine term is further expanded in a Taylor series and exponentiated

since the exponential term in the integrand will eliminate the oscillatory behavior of the cosine term:

$$\begin{aligned}\cos^2[Q(T) + Q(t) - Q(T+t)] &\approx \cos^2[(\lambda/\hbar)(1 - M(T)/M(0))t] \\ &\approx 1 - (\lambda/\hbar)^2(1 - M(T)/M(0))^2t^2 + ... \\ &\approx \exp[-(\lambda/\hbar)^2(1 - M(T)/M(0))^2t^2] = \exp[-f(T)t^2]\end{aligned}$$

where M(t) is defined as

$$M(t) = \int_0^\infty d\omega\ \omega^2 \coth(\hbar\omega\beta/2)\rho(\omega)\cos\omega t \qquad (19)$$

and $f(t)$ is defined as $f(t) = (\lambda/\hbar)^2[1 - M(t)/M(0)]^2$. The remaining integral is then a Gaussian, so the photon echo signal can be approximately written as

$$S_{PE}(\tau,T) \propto \frac{\sqrt{\pi}}{2\sqrt{A(\tau,T)}} \exp\left\{-2P(\tau) - \Delta_{in}{}^2\tau^2 + \frac{B(\tau,T)^2}{4A(\tau,T)}\right\} \times \left[1 + \mathrm{erf}\left(\frac{B(\tau,T)}{2\sqrt{A(\tau,T)}}\right)\right] \qquad (20)$$

where the auxiliary functions, $A(\tau,T)$ and $B(\tau,T)$, are defined as

$$A(\tau,T) = \langle\omega^2 \coth(\hbar\omega\beta/2)\rangle_\rho + \Delta_{in}{}^2 + M(T) - M(\tau+T) + f(T) \qquad (21.a)$$

$$B(\tau,T) = 2\Delta_{in}{}^2\tau + 2\dot{P}(\tau + T) - 2\dot{P}(T) \qquad (21.b)$$

erf( ) is the error function. $\dot{P}(t)$ is the derivative of $P(t)$. $\langle\ \rangle_\rho$ denotes an average over the spectral density, e.g.,

$$\langle\omega^2 \coth(\hbar\omega\beta/2)\rangle_\rho = \int_0^\infty d\omega\ \omega^2 \coth(\hbar\omega\beta/2)\rho(\omega)$$

In eq 20 there are two distinctive contributions, one is the exponential part and the other the terms inside the square bracket. The exponential part corresponds to the dephasing process, which is a monotonically decaying function with respect to the optical coherence time τ. In contrast, the term inside the square bracket is a monotonically increasing function approaching a finite value. The latter contribution describes the imperfect nature of the rephasing process induced by the Gaussian behavior of the short-time bath dynamics.

We next present some numerical calculations of the results, eqs 20 with 21. To this end, we assume a model spectral density whose functional form is

$$\rho(\omega) \propto (1/\omega)\exp(-\omega/\omega_c) \qquad (22)$$

where the cut-off frequency ω_c is assumed to be 40 cm^{-1}. To properly scale the spectral density, we assume that the mean square fluctuation amplitude, $\langle\omega^2 \coth(\hbar\omega\beta/2)\rangle_\rho$, at room temperature is 84 200 cm^{-2}, that is, $\langle\omega^2 \coth(\hbar\omega\beta/2)\rangle_\rho{}^{1/2}$ is about 290 cm^{-1}. This corresponds to the case when the reorganization energy λ is about 200 cm^{-1} at room temperature in the classical limit. Here $\langle\omega^2 \coth(\hbar\omega\beta/2)\rangle_\rho{}^{1/2}$ is approximately identical to the homogeneous broadening width of the absorption spectrum. Note that one can use the solvation reorganization energy for the reference parameter to scale the spectral density as discussed in section III. The spectral density given above will be used for the numerical calculations throughout this paper.

In Figure 3a, the exact numerical calculation of the integrated photon echo signal eq 17 with respect to the first delay time τ (dashed curve) is compared with the approximate photon echo signal, eq 20 (solid curve). Although there are slight deviations in the absolute magnitude as well as the decaying pattern in the longer time region, the agreement between the two is very much acceptable. As the second delay time T increases from 0 to 400 fs, the echo peak shift decreases progressively as shown in Figure 3b. In this calculation, the inhomogeneous width is assumed to be zero, so the echo peak shift approaches zero in this case (see section V for a detailed discussion on the asymptotic value of the echo peak shift as a function of the inhomogeneous width). In practice, by measuring the mirror image photon echo signal with wave vector of $\mathbf{k}_3 - \mathbf{k}_2 + \mathbf{k}_1$, one can measure the echo peak shift with very high precision.[28]

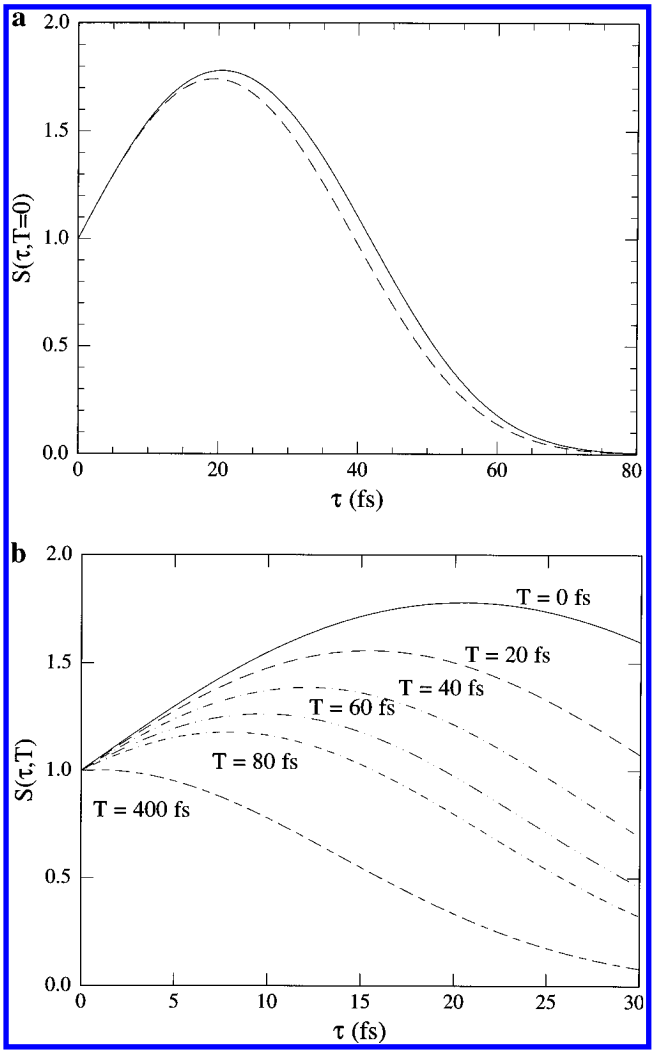

Figure 3. (a) The normalized integrated photon echo signals at $T = 0$ calculated by using eqs 17 (dashed curve) and 20 (solid curve). (b) For the second delay time $T = 0$, 20, 40, 60, 80, and 400 fs, the short-time photon echo signals are calculated from eq 20. The inhomogeneous width is assumed to be zero. The model spectral density used throughout this paper is given in the text (see eq 22). It should be noted that the echo peak shift decreases as the second delay time T increases.

The calculated echo peak shift as a function of the second delay time, T, is presented in Figure 4, where the solid dots and curve are the numerical results from eqs 17 and 20, respectively. Again the approximate echo signal, eq 20, is in good quantitative agreement with the exact numerical results from eq 17 for arbitrary inhomogeneous width: in Figure 4 the inhomogeneous width Δ_{in} is assumed to be 0 and 400 cm^{-1}, respectively. Although the decaying patterns of the echo peak shift are similar regardless of the inhomogeneous width, the asymptotic value of the echo peak shift when there is no static inhomogeneous contribution is zero as can be seen in Figure

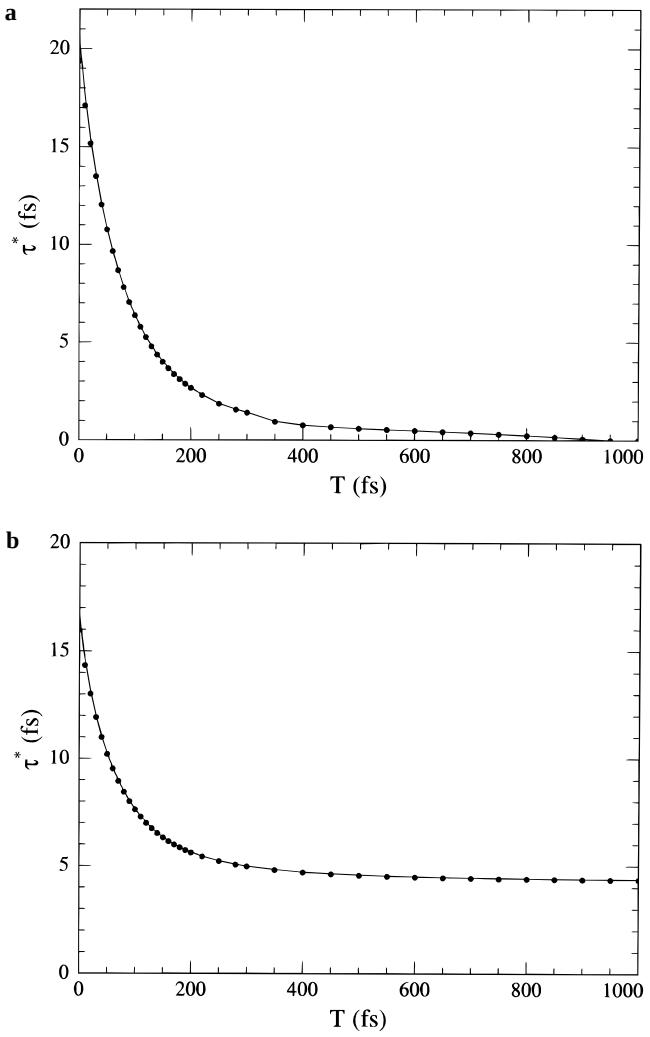

Figure 4. Echo peak shifts calculated by using Eqs 17 (solid dots) and 20 (solid curve). Panels a and b correspond to the cases when the inhomogeneous width Δ_{in} is 0 and 400 cm^{-1}, respectively.

4a, whereas that of the echo peak shift when Δ_{in} is 400 cm^{-1} (see Figure 4b) is finite. We discuss the inhomogeneous-width-dependent asymptotic echo peak shift in the following section. Here it should be emphasized that both eqs 17 and 20 are obtained on the basis of the impulsive approximation to the external optical pulses. Therefore, one may have to convolute the approximate signal with finite width pulses to make a quantitative comparison to the experimental data. This effect has been explored elsewhere.[28]

V. Photon Echo Peak Shift and Its Connection to Solvation Dynamics

As briefly mentioned in the Introduction, the echo peak shift, as shown in Figure 3, has been experimentally observed and numerical modeling suggested that the echo peak shift with respect to the second delay period in the three-pulse photon echo is closely related to the solvation correlation function. In this section we show that the echo peak shift as a function of T is indeed directly proportional to the solvation correlation function $S(t)$ in the long-time region.

A. Small Inhomogeneous Broadening Limit, $\Delta_{in}^2 \ll \langle \omega^2 \coth(\hbar\omega\beta/2)\rangle_\rho$. This is the case when the static inhomogeneous broadening is much smaller than the homogeneous one. Perhaps most liquids belong to this limit.

We first consider the echo peak shift $\tau^*(T)$ as a function of the second delay time. The approximate photon echo signal, eq 20, can be expanded with respect to the first delay time τ up to the second-order terms. It should be noted that in a typical polar liquid the echo peak shift is generally less than 10−15 fs. Therefore, the short-time expansion of the signal with respect to τ is well-justified. The maximum of the signal with respect to τ is found by setting the first derivative of the expanded signal equal to zero. Then the echo peak shift τ^* can be approximated as

$$\tau^*(T) = \frac{M(T)}{\sqrt{\pi}\langle \omega^2 \coth(\hbar\omega\beta/2)\rangle_\rho \sqrt{\langle \omega^2 \coth(\hbar\omega\beta/2)\rangle_\rho + f(T)}} \quad (23)$$

To obtain eq 23, we take only terms that are linear with respect to $M(T)$, though the denominator of the full expression includes $M(T)$ and other complicated functions of T. Therefore, we expect that the approximate equation 23 works well only in the longer time region, when $T \geq \tau_c$. Before we present a numerical calculation using eq 23, it is interesting to consider the high-temperature limit of eqs 23 with 19. In this limit one can replace $\coth(\hbar\omega/2k_BT)$ with $2k_BT/\hbar\omega$. From the definition of the reorganization energy λ in eq 12 and the fluorescence Stokes shift function $S(t)$ in eq 11, the echo peak shift τ^* can be rewritten as

$$\tau^*(T) = \frac{S(T)}{\sqrt{\pi[\Gamma + f(T)]}} \quad (24)$$

with

$$\Gamma \equiv \frac{2\lambda}{\hbar^2\beta} \quad (25)$$

Equation 24 shows how the echo peak shift is related to the solvation dynamics via the fluorescence Stokes shift (solvation) function $S(t)$ in the long-time region. The proportionality constant is the root mean square fluctuation amplitude. Once the normalized FSS function $S(T)$ is known, it is possible to obtain the magnitude of the bath fluctuation amplitude from eq 25 in the long-time region. Furthermore it is worth noting that, since $S(T)$ decays to zero as T increases, the asymptotic value of the echo peak shift τ^* vanishes in this case of a small inhomogeneous broadening limit. Inversely, if the echo peak shift approaches a finite value, one can exclude the small inhomogeneous broadening limit.

In Figure 5, a comparison of the numerically calculated echo peak shifts from both eq 20 (solid dots) and eq 24 (solid curve) is presented. Because of the approximations mentioned above, there is a large deviation between the two curves in the short-time region, i.e., for times less than the bath correlation time, but after 100 fs, which is approximately equal to the bath correlation time, the agreement is quantitative. This shows that the echo peak shift measurements can be used for the study of solvation dynamics.

In this small inhomogeneous broadening limit, the absorption spectrum is completely determined by dynamical processes, once the high-frequency vibrational levels are known. In this case, one can measure the line-shape function directly from the free induction decay.

B. Intermediate Inhomogeneous Broadening Limit, $\Delta_{in}^2 \leq \langle \omega^2 \coth(\hbar\omega\beta/2)\rangle_\rho$. When the inhomogeneous width is comparable to the dynamical width that is determined by the mean square root fluctuation amplitude, it is difficult to obtain approximate expressions for the form of the echo intensity profile from eq 20. However, photon echo peak shift measure-

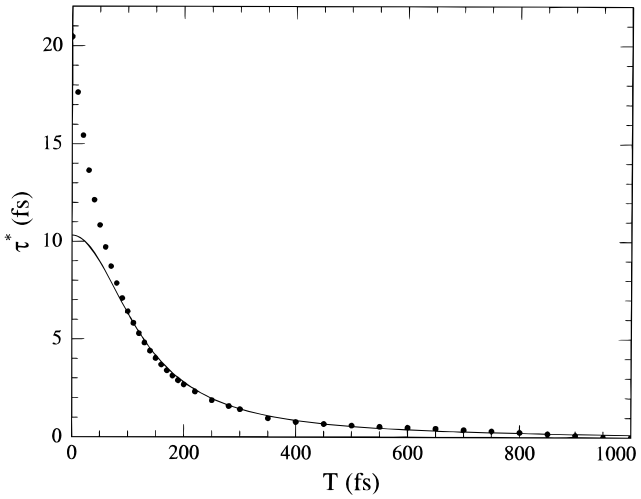

Figure 5. The echo peak shift as a function of the second delay time, T, is shown for a homogeneous system ($\Delta_{in} = 0$). The solid dots and curve correspond to those calculated from eq 20 with 21 and predicted with eq 23 with 19, respectively. For the given spectral density (eq 22), eq 23 is quantitatively identical to eq 24, that is, the classical limit of eq 23 at 300 K.

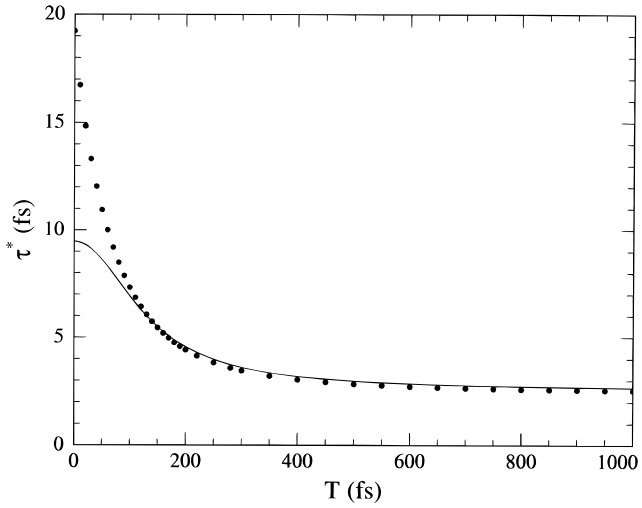

Figure 6. The echo peak shift as a function of the second delay time, *T*, shown for an intermediate inhomogeneous broadening case ($\Delta_{in} = 200$ cm^{-1}). The solid dots and curve correspond to those calculated from eq 20 with 21 and predicted with eq 26 with 19, respectively. The echo peak shift in this case approaches an asymptotic value determined by eq 27.

ments can still be an effective tool for studying the solvation dynamics or spectral diffusion of molecules dissolved in organic polymer glasses or chromophores in proteins, for example. By following the same procedure described in section IV.A, we find that the echo peak shift is approximately given by

$$\tau^*(T) = \left\{ [M(T) + \Delta_{in}{}^2] \sqrt{\langle \omega^2 \coth(\hbar\omega\beta/2)\rangle_\rho + \Delta_{in}{}^2 + f(T)} \right\} \Big/ \{\sqrt{\pi}[\langle \omega^2 \coth(\hbar\omega\beta/2)\rangle_\rho (\langle \omega^2 \coth(\hbar\omega\beta/2)\rangle_\rho + 2\Delta_{in}{}^2 + f(T)) + \Delta_{in}{}^2 f(T)]\} \quad (26)$$

where $M(T)$ was defined in eq 19. If the inhomogeneous width is set to zero, eq 26 reduces to the small inhomogeneous broadening limit, eq 23. In contrast to eq 23, as T increases the echo peak shift τ^* approaches a finite value,

$$\tau^*(T\rightarrow\infty) = \left[\Delta_{in}{}^2 \sqrt{\langle \omega^2 \coth(\hbar\omega\beta/2)\rangle_\rho + \Delta_{in}{}^2 + (\lambda/\hbar)^2} \right] \Big/ \{\sqrt{\pi}[\langle \omega^2 \coth(\hbar\omega\beta/2)\rangle_\rho (\langle \omega^2 \coth(\hbar\omega\beta/2)\rangle_\rho + 2\Delta_{in}{}^2 + (\lambda/\hbar)^2) + \Delta_{in}{}^2 (\lambda/\hbar)^2]\} \quad (27)$$

Therefore, the observation of the non-zero asymptotic value of the echo peak shift can provide strong evidence showing that there is a finite inhomogeneous contribution to the optical spectrum.

Except perhaps for water, at room temperature, most liquids, polymer glasses, and proteins belong to the classical limit, since twice the thermal energy is about 400 cm^{-1} and the distributions of the spectral densities of most of liquids are significantly less than 400 cm^{-1}. Therefore it is useful to consider the classical limits of eqs 26 and 27,

$$\tau^*(T) = \frac{\sqrt{\Gamma + \Delta_{in}{}^2 + f(T)}(\Gamma S(T) + \Delta_{in}{}^2)}{\sqrt{\pi}[\Gamma(\Gamma + 2\Delta_{in}{}^2 + f(T)) + \Delta_{in}{}^2 f(T)]} \quad (28)$$

$$\tau^*(T\rightarrow\infty) = \frac{\Delta_{in}{}^2 \sqrt{\Gamma + \Delta_{in}{}^2 + (\lambda/\hbar)^2}}{\sqrt{\pi}[\Gamma(\Gamma + 2\Delta_{in}{}^2 + (\lambda/\hbar)^2) + \Delta_{in}{}^2 (\lambda/\hbar)^2]} \quad (29)$$

where Γ was defined in eq 25. Equation 28 should be useful in describing the echo peak shift measured in various systems at room temperature in the intermediate inhomogeneous broadening case. At lower temperature, eq 26 should be used to interpret the echo peak shift with respect to the population delay, *T*. In this low-temperature regime, however, a clear physical picture, such as the direct connection to the solvation correlation function as shown by eq 28, is lost.

When the inhomogeneous width, Δ_{in}, is 200 cm^{-1}, the echo peak shift is numerically calculated as a function of the second delay time T (see Figure 6). As in the case of the small inhomogeneous broadening limit, the approximate expression eq 26 is in good agreement with the exact numerical results, though in the short-time (less than the bath correlation time) region the two curves do not match well.

One interesting application of the results obtained above is that the inhomogeneous width can be determined from eq 29 after measuring the asymptotic value of the echo peak shift, provided that the homogeneous root mean square fluctuation amplitude, Γ, from the FSS is known. This procedure should be useful in separately estimating the inhomogeneous and the homogeneous contributions in the intermediate inhomogeneous broadening limit.

It should be noted that the asymptotic peak shift expression, eq 27, is valid only when the dynamical coupling constant is larger than the inhomogeneous width, i.e., $\Delta_{in}{}^2 \leq \langle \omega^2 \coth(\hbar\omega\beta/2)\rangle_\rho$. The behavior of the asymptotic peak shift from exact numerical calculations is compared with the approximate result in Figure 7. In this figure, the root mean square fluctuation amplitude, $\langle \omega^2 \coth(\hbar\omega\beta/2)\rangle_\rho{}^{1/2}$, is fixed at 290 cm^{-1}, and the inhomogeneous width Δ_{in} is varied up to 1000 cm^{-1}. The approximate asymptotic peak position agrees with the exact numerical calculation up to an inhomogeneous width of 200 cm^{-1} after which the two curves begin to diverge. This failure is due to the fact that the error function in eq 20 is approximated to be a linear function for small arguments to obtain eq 26.

The exact form of the peak shift as a function of Δ_{in} shows that there are two values of Δ_{in} compatible with a given peak shift. However, as Figure 7 shows, the dependence of τ^* on Δ_{in} is very asymmetric and it will often be possible to rule out the large value of Δ_{in} as being inconsistent with the width of the absorption spectrum. Past the peak in the τ^* *vs* Δ_{in} plot,

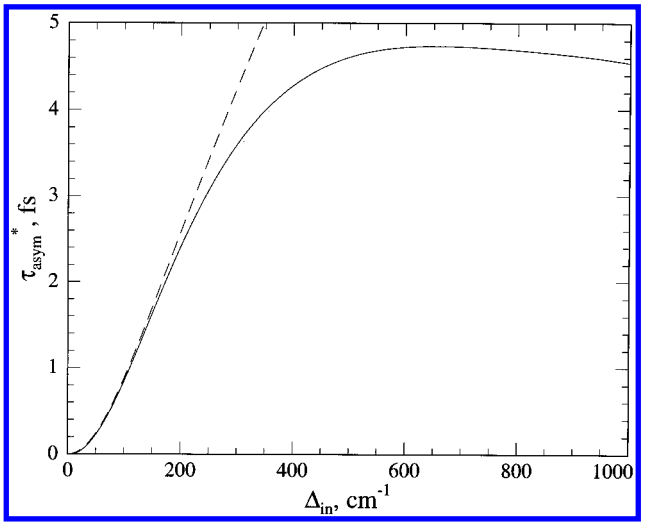

Figure 7. The asymptotic peak shift calculated as a function of Δ_{in} using eq 27, dashed curve, is compared with the asymptotic peak shift value obtained from eq 17, solid curve.

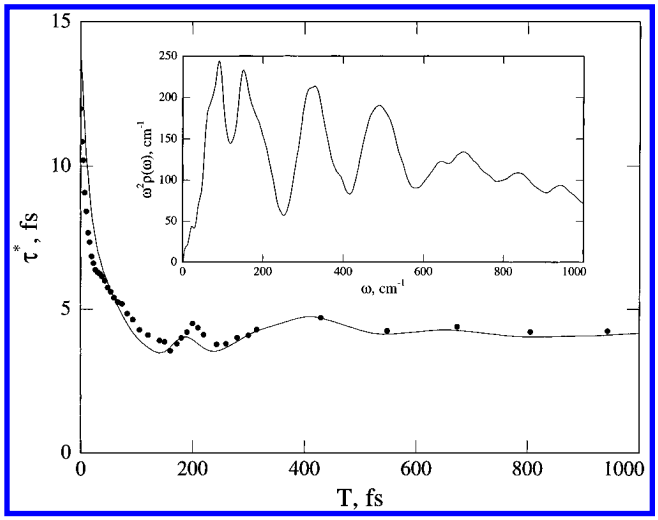

Figure 8. Experimental and calculated echo peak shifts of IR144 in a room temperature glass, PMMA, shown by the solid circles and the solid curve, respectively. The inset shows the normalized spectral density (see text for details).

the very weak dependence of τ^* on Δ_{in} will make it difficult to determine Δ_{in} accurately.

C. Large Inhomogeneous Broadening Limit, $\Delta_{in}^2 \gg \langle \omega^2 \coth(\hbar\omega\beta/2)\rangle_\rho$. When the inhomogeneous width is much larger than the root mean square fluctuation amplitude, the rephasing is perfect since the memory of the electronic phase associated with the static inhomogeneity is completely preserved during the second delay time. Therefore the echo field peaks at $t = \tau$ after the last pulse. This limit can be applied to the case when impurity chromophores are dissolved in glasses with broad distribution of the local environments. In this case the echo signal solely represents the homogeneous dephasing process, from eqs 20 and 21,

$$S_{PE}(\tau,T) \propto \exp[-2P(\tau)] \tag{30}$$

which is valid when $\tau \geq \Delta_{in}^{-1}$. Furthermore, the echo peak shift is zero regardless of the second delay time T. This is in contrast to the small inhomogeneous broadening limit, where the echo peak shift is observed as discussed in section V.A. On the basis of the discussion given above, one can conclude that, provided that the large value of Δ can be eliminated, *the existence of the asymptotic echo peak shift means that the inhomogeneous width is comparable to or smaller than the homogeneous width determined by the mean square root fluctuation amplitude, that is* $\Delta_{in}^2 \approx \langle \omega^2 \coth(\hbar\omega\beta/2)\rangle_\rho$ *or* $\Delta_{in}^2 \leq \langle \omega^2 \coth(\hbar\omega\beta/2)\rangle_\rho$. In other words, the traditional interpretation of the photon echo signal, that the photon echo signal is purely determined by the homogeneous dephasing process without any inhomogeneous contribution, is not correct as long as the asymptotic echo peak shift is non-zero. Note that the echo signal in this large inhomogeneous broadening limit does not depend on the second delay time T, which can be understood from the fact that there is no memory loss of the electronic phase induced by the static local environment during the second delay time. We shall not discuss this case further, since this limit has been studied extensively.[29,30,34]

Finally we emphasize again that the asymptotic echo signal $S_{PE}(\tau,T\rightarrow\infty)$, eq 20, in the small inhomogeneous broadening limit is formally identical to the echo signal, eq 30, in the large inhomogeneous broadening limit. In other words, in cases of small and large inhomogeneous broadening limits, the homogeneous contribution to the optical dephasing process, that is represented by the real part of the line-shape function as eqs 20 and 30, can be measured by using the conventional three-pulse photon echo experiment. On the other hand, in the case of the intermediate inhomogeneous broadening limit, one should use the echo peak shift measurements to obtain the solvation dynamics that are in turn related to the line-shape function as discussed in section III. Of course, the echo profile can be fitted using a numerical fitting procedure regardless of the inhomogeneous width, but it will be very difficult to find all of the parameters with confidence.

VI. Experimental Result and Numerical Calculations of the Line-Shape Function

To illustrate the use of the expressions developed above, we present a preliminary analysis of the dynamical and static contributions to the line broadening of IR144 in a room temperature glass, PMMA. A full analysis including temperature dependence will be presented elsewhere.[37]

The parameters required to fit the three-pulse echo peak shift data (solid circles in Figure 8) are the mean square fluctuation amplitude, Γ ($=2\lambda k_B T/\hbar^2$) and Δ_{in}. The procedure to obtain the spectral density and line-shape function is as follows.

(i) To obtain the spectral density, the time-dependent portion of the echo peak shift, $\tau^*(T) - \tau^*(\infty)$, is Fourier transformed. This assumes that the echo peak shift without the asymptotic peak shift is linearly proportional to $M(t)$ as shown in eq 23. The time dependence of $f(T)$ is ignored under the assumption that contribution from $f(T)$ will be smaller than the sum of Γ and Δ_{in}^2. The Fourier-transformed peak shift is divided by $\omega^2 \coth[\hbar\omega/2k_BT]$ to obtain the unscaled spectral density.

(ii) Since the echo peak positions are constant beyond $T = 1$ ps (scans were taken out to 200 ps) and since the asymptotic peak position does not depend on $S(t)$, photon echo signals at $T = 1$ ps are iteratively calculated by varying Γ and Δ_{in} until the peak position of the calculated signal matches the experimental peak shift value at $T = 1$ ps to obtain the correct Γ and Δ_{in}. The full set of response functions and 22 fs pulses are used for this calculation. The obtained values are $\Gamma = 240\ 100$ cm^{-2}, $\lambda = 580$ cm^{-1}, $\Delta_{in} = 400$ cm^{-1}. By using eq 12, the spectral density can be properly normalized and is shown in the inset of Figure 8.

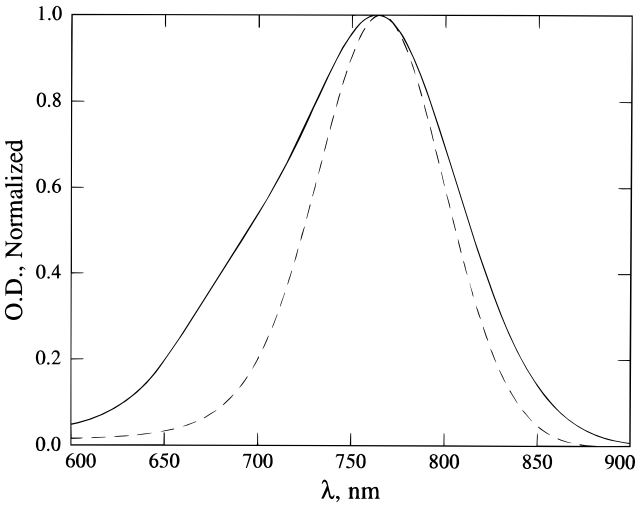

Figure 9. The absorption spectrum (dashed curve) calculated by using an inhomogeneous width of 400 cm^{-1} and the line-shape function compared with the experimentally measured spectrum (solid curve) for IR144 in PMMA at room temperature.

(iii) From the spectral density and the inhomogeneity width obtained by i and ii, the absorption spectrum can be calculated with

$$\sigma_A(\omega) \propto \mathrm{Re}\left[\int_{-\infty}^{\infty} dt \exp\{-i(\omega - \Omega)t\} \times \exp\left\{-\frac{\Delta_{in}^2 t^2}{2} - g(t)\right\}\right]$$

A comparison of calculated and experimental absorption spectra is shown in Figure 9. Reasonable agreement is obtained on the low-energy side of the spectrum. The poor agreement on the high-energy side most likely arises from underestimating the contribution of high frequency modes which were not impulsively excited by our 22 fs pulses. A more detailed analysis will be presented elsewhere.[37]

Equation 28 shows that $S(t)$ can be obtained directly from the peak shift by removing the $\tau^*(T\rightarrow\infty)$ value and normalizing for the amplitude. The $S(t)$ obtained in this manner will not be correct at short times since the peak shift measurements cannot correctly determine the initial decay of $S(t)$ as shown in Figures 5 and 6, but slower components will be described correctly. To demonstrate the utility of this approach, the echo peak shift $\tau^*(T)$ was recalculated using the above parameters and a pulse width of 22 fs using the full set of response functions.[30] The result is compared with the experimental data in Figure 8. The calculated initial peak shift is too large as mentioned above; however, the rest of the curve and in particular the long-time behavior are well-reproduced. Thus, an initial guess of the form of $S(t)$ and other parameters can be obtained through this method. These parameters can be used to fit the experimental data once the initial part of $S(t)$ is correctly adjusted.[37]

VII. Summary

In general, nonlinear spectroscopies can be completely described once the nonlinear response functions are known.[29] Furthermore, the nonlinear response functions were shown to be expressed by a combination of the line-shape functions, $g(t)$.[30,32] We first established the relationship between the solvation function, the fluorescence Stokes shift function $S(t)$, and the line-shape function by defining the spectral density as eq 9. One can use various methods, for example, fluorescence Stokes shift measurements, computer simulations, or analytical theories, to obtain the spectral density of a given solvent. Then using the relationships given in this paper, one can easily calculate various nonlinear spectroscopic signals. Inversely, using the nonlinear spectroscopic methods, particularly the photon echo peak shift measurement, it is possible to obtain information on the solvation dynamics. The latter approach was taken in this paper.

Considering the conventional integrated photon echo in the impulsive limit, we obtained the approximate echo signal in eq 20. In the small or intermediate inhomogeneous broadening limits, we further showed that the echo peak shift as a function of the second delay time is directly proportional to the fluorescence Stokes shift function for times greater than the bath correlation time. By using the echo shift formula developed in this paper, an analysis of the echo shift data of IR144 in PMMA at room temperature was presented. It was found that the inhomogeneous width is approximately 400 cm^{-1}. The chromophore−solvent spectral density of this composite system was obtained by Fourier transform of the echo shift.

We conclude by emphasizing that the theoretical description given in this paper does not depend on any specific bath model such as the multimode Brownian oscillator model or the effective harmonic oscillator bath model. Therefore, from photon echo experiments and the interpretation procedures discussed in this paper, one can test the validities of various theoretical models directly and obtain bath response functions without relying on simplified models with adjustable parameters. Consequently, one can obtain the spectral density directly from photon echo experiments.

Acknowledgment. This work was supported by the National Science Foundation. M.C. thanks Prof. R. J. Silbey for his support. J.-Y.Yu was partly supported by a Department of Education GAANN Fellowship, and Y.N. thanks JSPS for a Fellowship.

References and Notes

(1) Stoneham, A. M. *Rev. Mod. Phys.* **1969**, *41*, 82.
(2) *Persistent Spectral Hole-Burning: Science and Applications*; Moerner, W. E., Ed.; Springer-Verlag: Berlin, 1988.
(3) Mossberg, T. W.; Kachru, R.; Flusberg, A. M.; Hartmann, S. R. *Phys. Rev.* **1979**, *A20*, 1976. Gordon, J. P.; Wang, C. H.; Patel, C. K. N.; Slusher, R. E.; Tomlinson, W. J. *Phys. Rev.* **1969**, *179*, 294. Schoemaker, R. L. *Annu. Rev. Phys. Chem.* **1979**, *30*, 239.
(4) Mossberg, T.; Flusberg, A.; Kachru, R.; Hartmann, S. R. *Phys. Rev. Lett.* **1977**, *39*, 1523. Lee, H. W. H.; Patterson, F. G.; Olson, R. W.; Wiersma, D. A.; Fayer, M. D. *Chem. Phys. Lett.* **1982**, *90*, 172.
(5) Hesselink, W. H.; Wiersma, D. A. *Phys. Rev. Lett.* **1979**, *43*, 1991. Hesselink, W. H.; Wiersma, D. A. *J. Chem. Phys.* **1980**, *73*, 648.
(6) Morsink, J. B. W.; Hesselink, W. H.; Wiersma, D. A. *Chem. Phys.* **1982**, *71*, 289. Saikan, S.; Nakabayashi, T.; Kanematsu, Y.; Imaoka, A. *J. Chem. Phys.* **1988**, *89*, 4609.
(7) Becker, P. C.; Fragnito, H. L.; Bigot, J. Y.; Brito-Cruz, C. H.; Fork, R. L.; Shank, C. V. *Phys. Rev. Lett.* **1989**, *63*, 505. Bigot, J. Y.; Portella, M. T.; Schoenlein, R. W.; Bardeen, C. J.; Migus, A.; Shank, C. V. *Phys. Rev. Lett.* **1991**, *66*, 1138.
(8) Nibbering, E. T. J.; Wiersma, D. A.; Duppen, K. *Phys. Rev. Lett.* **1991**, *66*, 2464.
(9) Joo, T.; Albrecht, A. C. *Chem. Phys.* **1993**, *176*, 233.
(10) Allen, L.; Eberly, J. H. *Optical Resonance and Two-Level Atoms*; Wiley: New York, 1975.
(11) Shen, Y. R. *The Principles of Nonlinear Optics*; Wiley: New York, 1984.
(12) Cho, M.; Stratt, R. M. *J. Chem. Phys.* **1994**, *100*, 6700.
(13) Maroncelli, M.; Fleming, G. R. *J. Chem. Phys.* **1988**, *89*, 5044. Maroncelli, M. *J. Chem. Phys.* **1991**, *94*, 2084. Carter, E. A.; Hynes, J. T. *J. Chem. Phys.* **1991**, *94*, 5961. Kumar, P. V.; Maroncelli, M. *J. Chem. Phys.* **1995**, *103*, 3038. Ladanyi, B. M.; Stratt, R. M. *J. Phys. Chem.* **1995**, *99*, 2502.
(14) Rosenthal, S. J.; Xie, X.; Du, M.; Fleming, G. R. *J. Chem. Phys.* **1992**, *95*, 4715.
(15) Horng, M. L.; Gardecki, J.; Papazyan, A.; Maroncelli, M. *J. Phys. Chem.* **1995**, *99*, 17311.
(16) Cho, M.; Scherer, N. F.; Fleming, G. R.; Mukamel, S. *J. Chem. Phys.* **1992**, *96*, 5618.

(17) Cho, M.; Fleming, G. R. *J. Phys. Chem.* **1994**, *98*, 3478.
(18) de Boeij, W. P.; Pshenichnikov, M. S.; Wiersma, D. A. *Chem. Phys. Lett.* **1995**, *238*, 1. de Boeij, W. P.; Pshenichnikov, M. S.; Wiersma, D. A. *Chem. Phys. Lett.* **1995**, *247*, 264.
(19) Joo, T.; Jia, Y.; Fleming, G. R. *J. Chem. Phys.* **1995**, *102*, 4063.
(20) Vohringer, P.; Arnett, D. C.; Yang, T.-S.; Scherer, N. F. *Chem. Phys. Lett.* **1995**, *237*, 387.
(21) Pshenichnikov, M. S.; Duppen, K.; Wiersma, D. A. *Phys. Rev. Lett.* **1995**, *74*, 674.
(22) Bader, J. S.; Kuharski, R. A.; Chandler, D. *J. Chem. Phys.* **1990**, *93*, 230. Song, X.; Marcus, R. A. *J. Chem. Phys.* **1993**, *99*, 7768.
(23) Roy, S.; Bagchi, B. *J. Chem. Phys.* **1993**, *99*, 9938.
(24) Raineri, F. O.; Resat, H.; Perng, B.-C.; Hirata, F.; Friedman, H. L. *J. Chem. Phys.* **1994**, *100*, 1477.
(25) Neria, E.; Nitzan, A. *J. Chem. Phys.* **1992**, *96*, 5433.
(26) Bagchi, B.; Chandra, A. *J. Chem. Phys.* **1992**, *97*, 5126.
(27) Weiner, A. M.; De Silvestri, S.; Ippen, E. P. *J. Opt. Soc. Am. B* **1985**, *2*, 654. De Silvestri, S.; Weiner, A. M.; Fujimoto, J.; Ippen, E. P. *Chem. Phys. Lett.* **1984**, *112*, 195.
(28) Joo, T.; Jia, Y.; Yu, J.-Y.; Lang, M. J.; Fleming, G. R. *J. Chem. Phys.* **1995**, *104*, 6089.
(29) Mukamel, S. *Principles of Nonlinear Optical Spectroscopy*; Oxford: New York, 1995.
(30) Yan, Y. J.; Mukamel, S. *J. Chem. Phys.* **1991**, *94*, 179.
(31) Shemetulskis, N. E.; Loring, R. F. *J. Chem. Phys.* **1992**, *97*, 1217.
(32) Mukamel, S. *Annu. Rev. Phys. Chem.* **1990**, *41*, 647.
(33) Adelman, S. A. *Adv. Chem. Phys.* **1980**, *44*, 143.
(34) Cho, M.; Fleming, G. R. *J. Chem. Phys.* **1993**, *98*, 2848.
(35) Landau, L. D.; Lifshitz, E. M. *Statistical Physics, Part I*, 3rd ed.; Pergamon: New York, 1980.
(36) Chandler, D. *Introduction to Modern Statistical Mechanics*; Oxford: New York, 1987.
(37) Nagsawa, Y.; Passino, S. A.; Joo, T.; Fleming, G. R. Manuscript in preparation.

JP9601983